JACS
JOURNAL OF THE AMERICAN CHEMICAL SOCIETY

ARTICLE

pubs.acs.org/JACS

# $V_2O_5$-Anchored Carbon Nanotubes for Enhanced Electrochemical Energy Storage

M. Sathiya,[†] A. S. Prakash,*[,†] K. Ramesha,[†] J−M. Tarascon,[‡] and A. K. Shukla[§]

[†]CSIR Central Electrochemical Research Institute-Chennai Unit, CSIR-Madras Complex, Taramani, Chennai-600 113, India

[‡]Laboratoire de Réactivité et Chimie des Solides, CNRS UMR 6007, 33, rue Saint Leu − Université de Picardie Jules Verne, 80039 Amiens, France

[§]Solid State and Structural Chemistry Unit, Indian Institute of Science, Bangalore-560 012, India

Supporting Information

**ABSTRACT:** Functionalized multiwalled carbon nanotubes (CNTs) are coated with a 4−5 nm thin layer of $V_2O_5$ by controlled hydrolysis of vanadium alkoxide. The resulting $V_2O_5$/CNT composite has been investigated for electrochemical activity with lithium ion, and the capacity value shows both faradaic and capacitive (nonfaradaic) contributions. At high rate (1 C), the capacitive behavior dominates the intercalation as 2/3 of the overall capacity value out of 2700 C/g is capacitive, while the remaining is due to Li-ion intercalation. These numbers are in agreement with the Trasatti plots and are corroborated by X-ray photoelectron spectroscopy (XPS) studies on the $V_2O_5$/CNTs electrode, which show 85% of vanadium in the +4 oxidation state after the discharge at 1 C rate. The cumulative high-capacity value is attributed to the unique property of the nano $V_2O_5$/CNTs composite, which provides a short diffusion path for $Li^+$-ions and an easy access to vanadium redox centers besides the high conductivity of CNTs. The composite architecture exhibits both high power density and high energy density, stressing the benefits of using carbon substrates to design high performance supercapacitor electrodes.

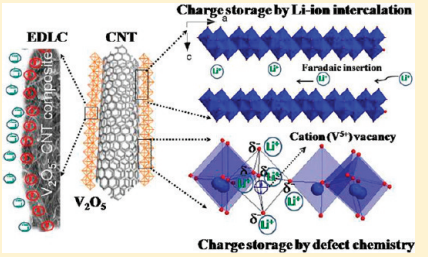


## INTRODUCTION

Energy is pervasive in nature and is one of the most pressing problems of the human kind. The growing energy demands of 21st century urge electrochemists to explore newer mechanisms for energy storage that far exceed current technologies. With this in view, new concepts in electrochemical energy storage that are superior to conventional energy storage devices are under intensive investigations. For instance, rechargeable Li-air batteries that can store at least 5 times excess charge than conventional secondary batteries[1−3] and pseudocapacitors (or ultracapacitors) that can store at least 10 times higher charge than conventional double layer capacitors have been reported.[4−6] Concomitantly, seminal advances in materials for batteries and capacitors have been made. For example, nanowires of Si are developed as Li-ion battery anode material with 3−5 times higher sustainable capacity than traditional graphite anodes.[7] Besides, conversion electrodes rather than classical insertion reactions are also being explored as anodes due to the staggering capacity gains.[8−10] On the other hand, high surface area transition metal oxides and composites with capacity values several times higher than double layer capacitance have also been investigated.[11,12] Capacitors have high power densities, whereas secondary Li-ion batteries exhibit high energy density; the combination of both offers an attractive approach to realize future devices reuniting attractive energy and power capabilities.[13,14] Indeed, the materials exhibiting charge storage using both capacitive and faradaic means are of great interest as witnessed in recent publications dealing with mesoporous transition metal oxides for energy storage.[15] Inspired by these studies, we have sought to revisit nano $V_2O_5$ that has been the subject of many studies (although sometimes contradictory) either as pseudocapacitive electrode material or as high capacity cathode material for lithium batteries or both. The purpose of this study, in particular, is to unravel the importance of growing nano-oxides on special substrates such as CNTs to enhance their charge-storage capability.

Crystalline $V_2O_5$ is known to have orthorhombic layered structure, wherein $VO_5$ square pyramids share adjacent corner and edges (see Figure S-1(a) of the Supporting Information).[16] On the other hand, quasi crystalline $V_2O_5$ xerogels comprising bilayers separated with a characteristic interlayer distance serve as a location for intercalating guest species. The bilayers comprise single $V_2O_5$ layers with edge and corner shared $VO_5$ square pyramid units (see Figure S-1(b) of the Supporting Information).[17] Accordingly, aerogels of $V_2O_5$ possess surface areas as high as 250 $m^2/g$ as compared to nanocrystalline $V_2O_5$, for which it ranges between a few $m^2/g$ and 50 $m^2/g$.[18] Despite their high surface area values, aerogels as such are poorly crystallized. In light of Dunn's recent study[15] demonstrating the benefits of combined mesoporous morphologies and crystallographically oriented film to enhance the energy and capacitive storage of oxides in general, the present study employs multiwalled carbon nanotubes as structure directing substrate for growing thin $V_2O_5$ layers.

**Received:** August 3, 2011
**Published:** September 02, 2011





dx.doi.org/10.1021/ja207285b | J. Am. Chem. Soc. 2011, 133, 16291–16299

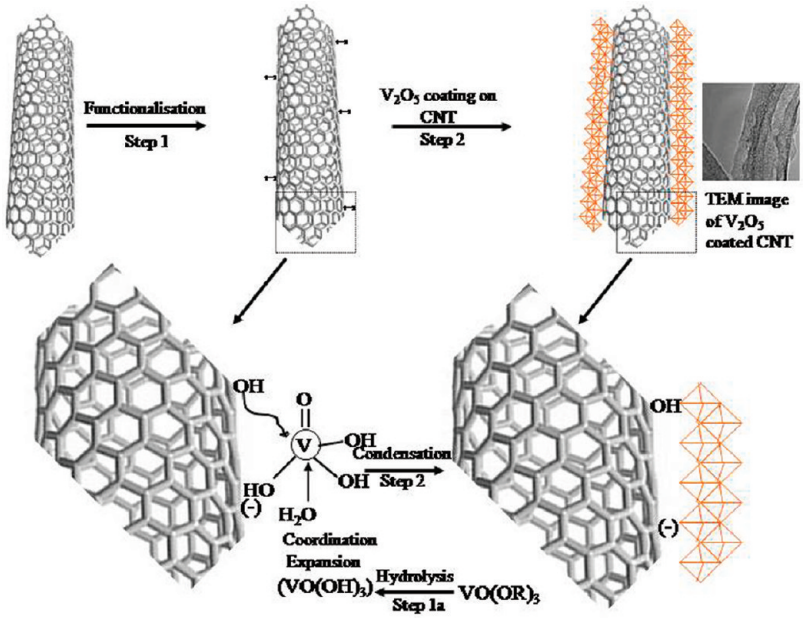


**Figure 1.** Schematic illustration for the synthesis and structure of $V_2O_5$/CNTs. The functionalization of carbon nanotubes in step 1 results in the modification of CNT surface with functional groups like −OH, $-COO^-$, −CO, etc. Vanadium alkoxide (VO $(OR)_3$) hydrolyzes to vanadium oxytrihydroxide $(VO(OH)_3)$ that undergoes coordination expansion with functional groups present on CNT surface as depicted by the inflated picture at the bottom followed by condensation to $V_2O_5$ layers grafted on CNTs.

## GRAFTING $V_2O_5$ LAYERS ON CNTs

Carbon nanotubes are one-dimensional nanomaterials with a huge aspect ratio that provides them with a unique combination of mechanical, electrical, and thermal properties.[19−21] Further, their ability to host other materials and to be used as hybrid nanostructures has received increased attention in recent years.[22] These hybrid nanostructures often possess interesting structural,[23] electrochemical,[24] electromagnetic,[25] and other properties that are otherwise not exhibited by their individual or bulk counterpart. In this context, the present study envisions one to use a few layers of $V_2O_5$ coated over CNTs as high performing battery hybrid supercapacitor electrode material.

Anchoring of $V_2O_5$ on the CNT surface is achieved as shown schematically in Figure 1. The strategy is to anchor a few layers of vanadium oxide over the functionalized carbon nanotube surface. Step 1 in Figure 1 shows the chemical fuctionalization of CNT surfaces using concentrated nitric acid that introduces functional groups such as hydroxyl, carboxyl, and carbonyl groups. These functional groups not only facilitate the dispersion of CNTs but also serve as centers for polymerization and condensation of vanadium oxy-trihydroxide formed during slow hydrolysis of vanadium oxy-tripropoxide (step 1a). Vanadium oxy-trihydroxide anchored via functional groups further undergoes coordination expansion through nucleophilic addition of water or hydroxyl groups.[26] Step 2 shows the condensation occurring through hydroxyl group (olation) and oxo-group (oxolation)[27] resulting in the grafting of $V_2O_5$ layers on CNT surface parallel to the CNT's basal carbon rings.

## RESULTS AND DISCUSSION

The X-ray diffraction pattern recorded for the as-prepared composite hybrid material is shown in Figure 2a. It comprises diffraction peaks corresponding to carbon (marked as "*") and $V_2O_5$ (marked with "#"). Vanadium pentoxide diffraction peaks indexable as monoclinic layered $C2/m$ space group with lattice parameters $a$ = 11.720 (5) Å, $b$ = 3.571 (2) Å, $c$ = 11.525(4) Å, and $\beta$ = 88.65° indicate that $V_2O_5$ anchored to CNTs retains the layered xerogel structure (see $V_2O_5$ xerogel structure in Figure S-1(b) of the Supporting Information). The scanning electron micrograph for $V_2O_5$/CNT composite is shown in Figure 2b. It is noteworthy that no segregation of $V_2O_5$ is seen in the micrograph.

The transmission electron micrograph shown in Figure 2c and the micrograph presented as inset confirm the uniform coating of $V_2O_5$ over CNTs as there are no extra $V_2O_5$ particles found agglomerated outside the CNT surfaces. The high-resolution image shown in Figure 2d elucidates the structural features of $V_2O_5$ growth onto CNTs. An examination of the interface of $V_2O_5$/CNT reveals that (−114) planes of $V_2O_5$ are epitaxially grown parallel to (002) planes of CNT over which (062) planes are oriented perpendicularly to (−114) planes (see Figure S-2 of the Supporting Information). The overall thickness of $V_2O_5$ layers found on a carbon nanotube is ∼4−5 nm.

The formation of $V_2O_5$ is further confirmed using X-ray photoelectron spectroscopy. Figure 3a shows survey-scan XPS for $V_2O_5$−CNT composite. The peaks corresponding to vanadium, oxygen, and carbon are seen along with peaks corresponding to silver that arise from silver paste used for sample mounting. Figure 3c shows the core level binding energy for V (2p) peaks. The binding energy for vanadium $2p_{3/2}$ and $2p_{1/2}$ observed, at 517.2 and 524.5 eV agree well with those of $V^{5+}$ in $V_2O_5$, respectively.[28] The corresponding O (1s) spectrum is shown in Figure 3d; the O (1s) spectrum is broad and asymmetric and could be deconvoluted into three peaks with realistic full width at half-maximum (fwhm) values, indicating the existence of three different oxygen species. The peak position at a binding energy of 530 eV is attributed to O (1s) of $V_2O_5$.[28]

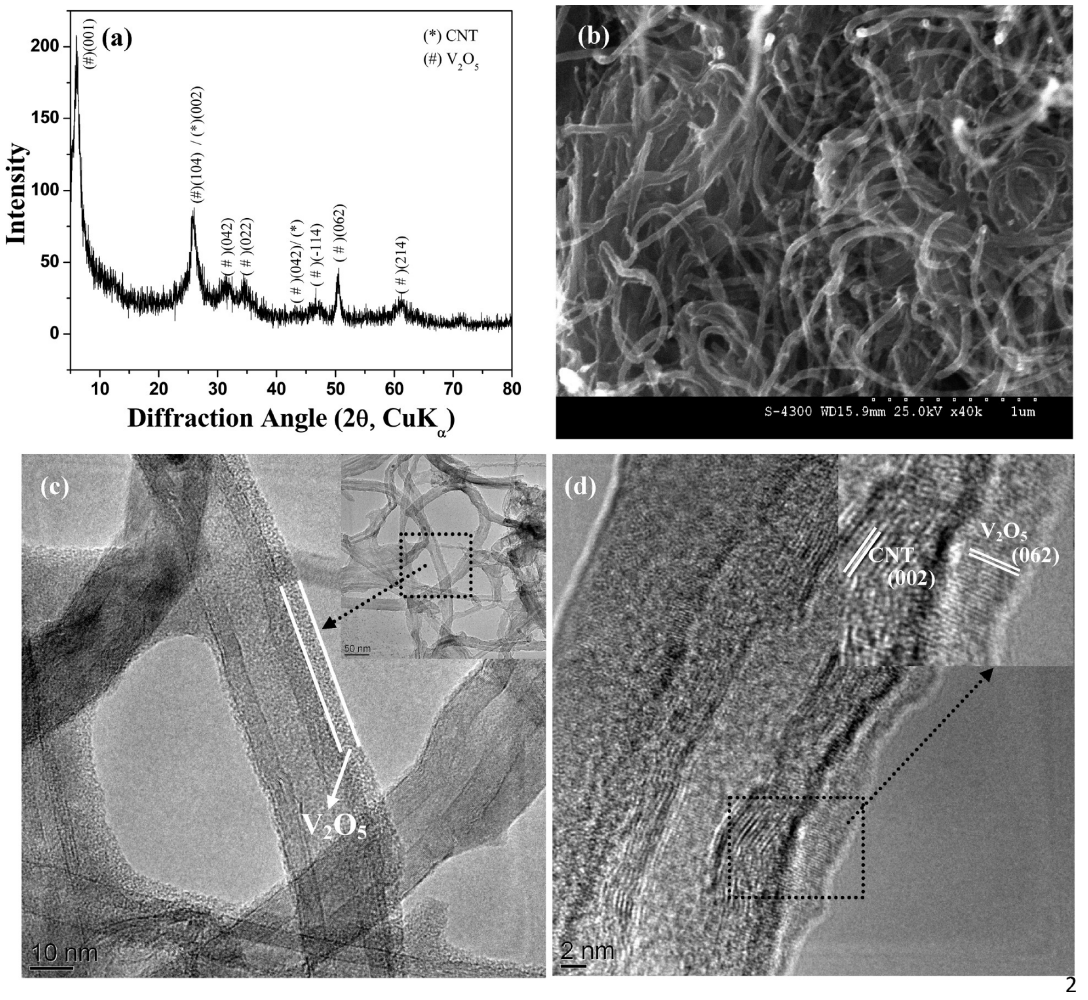


**Figure 2.** Structural and morphological characterization of $V_2O_5$/CNT composite. (a) Powder X-ray diffraction pattern recorded with Cu $K_\alpha$ radiation; the diffracted peaks marked with "#" correspond to $V_2O_5$, and peaks marked with "*" correspond to CNTs. (b) Scanning electron microscopy image showing the morphology of $V_2O_5$−carbon nanotube. (c) Transmission electron microscopy image showing the absence of $V_2O_5$ particles or agglomeration over CNT surface. (d) High-resolution TEM image showing lattice image of $V_2O_5$ with CNT lattice. Thin coating of about 4−5 nm thick $V_2O_5$ is marked on the micrograph.

Peaks at 531.5 and 534 eV are due to OH and $H_2O$ molecules, respectively.[29] The latter is probably from functionalized carbon nanotubes and adsorbed moisture over high surface area oxide. The C (1s) core-level spectra shown in Figure 3b can be deconvoluted into three peaks appearing at 284.4, 285.6, and 288 eV. The dominant peak at 284.4 eV is due to the $sp^2$-hybridized carbon atoms of the graphene sheets.[30] The peak at 285.6 eV can be assigned to carbon atoms singly coordinated to an oxygen atom as in phenols or ethers (C−OR). The small peak at 288 eV is attributed to the presence of carbonyl (C═O) groups.[30]

## ■ ELECTROCHEMICAL PERFORMANCE

To investigate the electrochemical behavior, Swagelok type cells of $V_2O_5$/CNT hybrid against lithium metal counter electrode are assembled and subjected to galvanostatic charge−discharge cycling. The cells with 2 mg/cm$^2$ of active material are cycled at a rate corresponding to the insertion or deinsertion of 1 mol Li/per mol of $V_2O_5$ in 2 h (C/2) in the voltage window between 1.5 and 4.0 V. Figure 4a shows the voltage−composition profile for a typical $V_2O_5$-anchored CNT cell. For comparison, the voltage−composition profile for $V_2O_5$ xerogels prepared under similar conditions but without the carbon nanotubes is shown in Figure 4b; corresponding plots of capacity as a function of cycle number are also shown as insets to the respective figures. Similarly, plots for bulk $V_2O_5$ obtained from a commercial source are shown in Figure 4c. The voltage−composition profile for $V_2O_5$-anchored CNTs is smooth and differs from crystalline $V_2O_5$ that shows characteristic plateaus corresponding to phase transitions in crystalline $V_2O_5$ with insertion of Li (see CV for crystalline $V_2O_5$ in Figure S-3 of the Supporting Information). By contrast, initially it resembles the voltage profile reported for $V_2O_5$ xerogels but with more Li uptake. During the first discharge, $V_2O_5$-anchored CNT composite electrode reacts with 6 mol of Li/mol of $V_2O_5$, resulting in a capacity value of 850 mAh/g, and the corresponding charge cycle is completely reversible; hereafter, all of the capacities and capacitances will be reported in per gram of $V_2O_5$, if not otherwise specified. By contrast, the reversible capacities for $V_2O_5$ xerogels and crystalline bulk phase are about 200 and 280 mAh/g, respectively; the capacity retention being better for the latter (5% drop after 25 cycles as compared to 40% for CNT−$V_2O_5$ composites). Surprisingly, the composite electrode exhibits at least 4-fold higher capacity than the


dx.doi.org/10.1021/ja207285b |J. Am. Chem. Soc. 2011, 133, 16291–16299

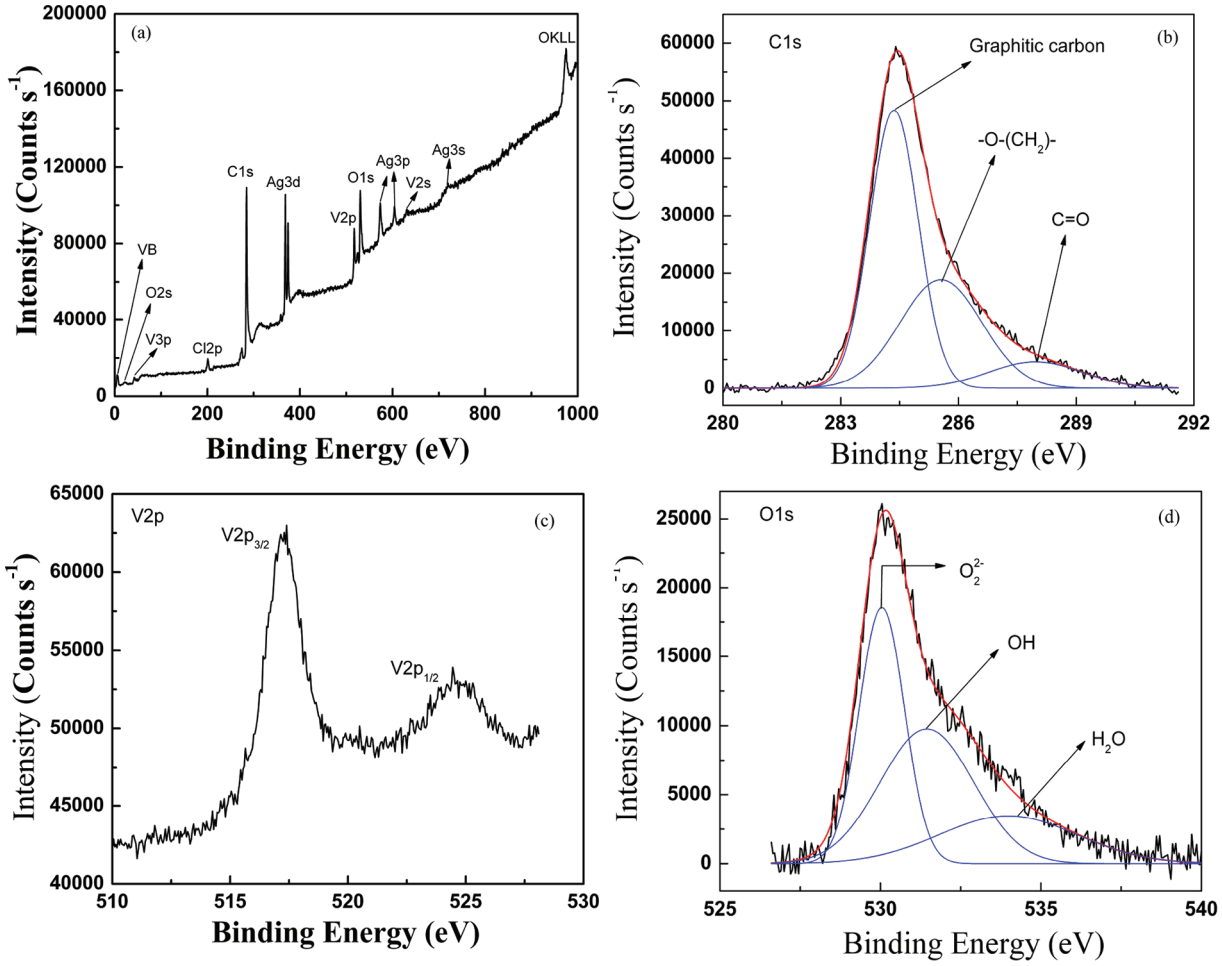


**Figure 3.** X-ray photoelectron spectrum for the $V_2O_5$/CNT surface. (a) Survey spectrum showing C (1s), V (2p), V (3p), and O (1s) emanating from the sample, and Ag (3d), Ag (3p), and Ag (3s) are due to silver paste used for fixing the sample over stub. (b) Deconvoluted C (1s) region of XP spectrum showing prominent carbon with graphitic nature, which comes from CNTs. The C (1s) intensity appears at higher binding energies originated from organic carbon of functional groups. (c) The V (2p) binding energy region showing spin orbit splitting of $2p_{3/2}$ and $2p_{1/2}$. (d) O (1s) region showing the prominent peak corresponding to the oxide ion of $V_2O_5$ layers and higher binding energy regions corresponding to the oxygen of functional groups and $H_2O$.

corresponding $V_2O_5$ xerogels. Such a remarkably high Li storage capacity reported earlier for $V_2O_5$ xerogels has been considered as quasi 2D-process because there are no associated phase changes during intercalation/deintercalation.[31,32] To further understand the unusually high Li-reactivity of $V_2O_5$-anchored CNT electrode, cyclic voltammetric experiments are conducted on $V_2O_5$-anchored CNT versus Li. It is noteworthy that uptake of 6 Li/mol of $V_2O_5$ has been reported with $V_2O_5$ aerogels,[33] but no explanation has been provided.

Figure 5a shows the cyclic voltammogram for $V_2O_5$-anchored CNTs at varying scan rates from 0.05 to 2 mV/s. The area under the curve represents the total stored charge originating from faradaic and nonfaradaic processes. It can be explained using the power law $i = a\nu^b$, where $\nu$ is the scan rate, and both $a$ and $b$ are adjustable parameters.[34] The parameter $b$ is determined from the slope of the linear plot of log $i$ versus log $\nu$ (see Supporting Information S-4). In general, slope $b = 1$ for surface redox reactions involving nondiffusion-controlled processes, thus $i = a\nu$. While for the ideal diffusion-controlled faradaic process, the slope $b = 1/2$ and satisfies Cottrell's equation: $i = a\nu^{1/2}$.[35]

Slope $b$ is obtained by plotting log $i$ versus log $\nu$ as a function of voltage, $V$ (see Supporting Information S-5). It is noteworthy that the slope is ~0.5 at peak potentials indicating the dominance of the diffusion-limited process to overall charge storage, whereas the slope value is ~1 at other potentials indicating contribution of redox pseudocapacitance to charge storage, with "pseudo" referring to a faradaic reaction that is not diffusion-controlled. Therefore, the current response "$i$" at a given potential, $V$, is the sum of two contributions arising from the redox pseudocapacitance and intercalation capacity as discussed below.

$$i(V) = a_1\nu + a_2\nu^{1/2}$$

or

$$i(V)/\nu^{1/2} = a_1\nu^{1/2} + a_2$$

where $a_1\nu$ and $a_2\nu^{1/2}$ correspond to the current contributions from the capacitive (redox pseudo capacitance plus double layer capacitance) and insertion processes, respectively. Thus, by determining $a_1$ and $a_2$ (see Supporting Information S-6), it is possible to determine the current response due to capacitive and insertion processes at a specific potential. In Figure 5b, the

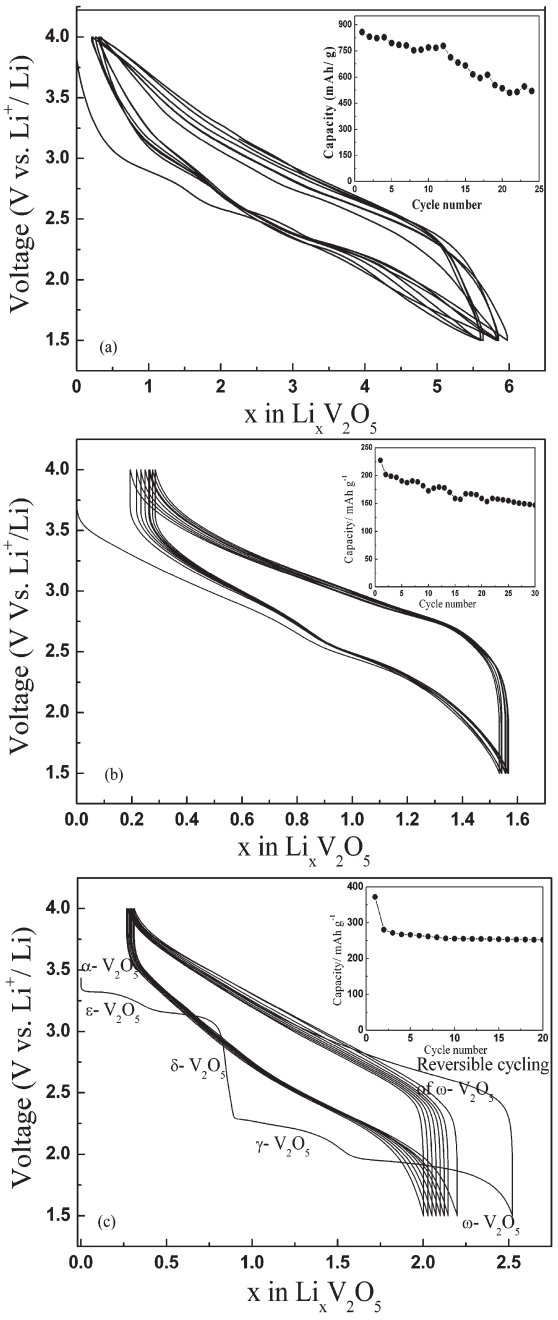


**Figure 4.** Galvanostatic cycling showing voltage−composition profile of different types of $V_2O_5$ samples versus Li cycled at $C/2$ (1Li in 2 h) rate in the voltage range of 1.5−4.0 V. (a) Voltage composition profile of $V_2O_5$ anchored CNT sample versus Li cell. (b) Voltage composition profile of $V_2O_5$ xerogel versus Li; $V_2O_5$ xerogel is prepared under identical condition but without the functionalized CNTs. (c) Voltage composition profile of commercially available crystalline $V_2O_5$ sample versus Li. The inset to each figure shows the corresponding plot of capacity retention as a function of cycle number.

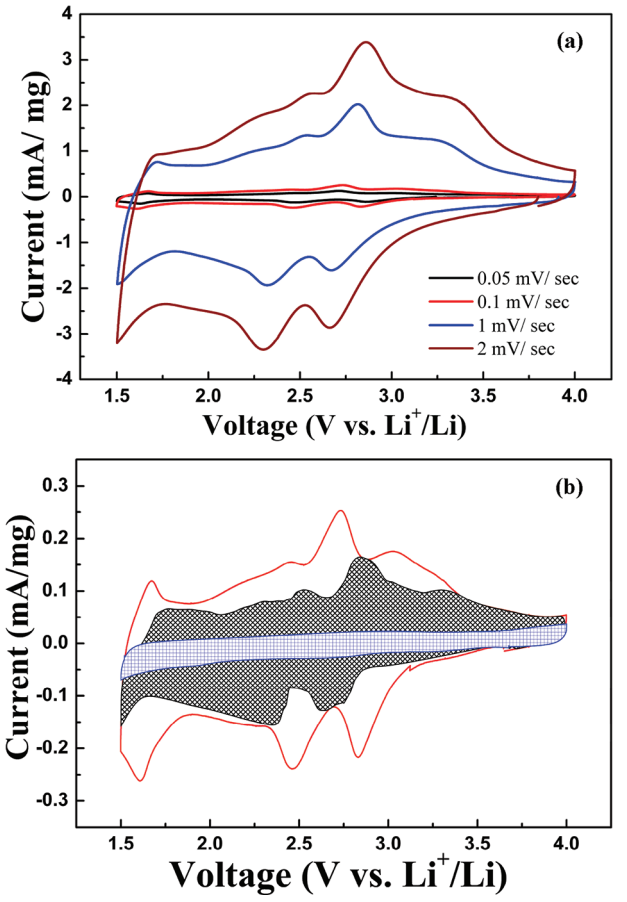


**Figure 5.** Potentiostatic cycling to understand the charge storage mechanism in $V_2O_5$/CNT electrodes. (a) Cyclic voltammograms at varying sweep rates for $V_2O_5$/CNT composite electrode versus Li cell with 1 M $LiClO_4$/EC-DMC electrolyte and (b) capacitive and diffusion-controlled charge storage contributions separated with cyclic voltammogram at 0.1 mV/s scan. The shaded area in blue corresponds to the cyclic voltammogram collected on a swagelok cell using bare CNTs in amount equal to what was used in our composite electrode. The gray shaded portion of the CV corresponds to capacitive contribution.

voltage profile for the capacitive current response is shown as a shaded area in comparison with the total measured current on a typical CV for $V_2O_5$-anchored CNT at the scan rate of 0.1 mV/s. It is apparent from these data that maximum Li insertion capacity, that is, the diffusion-controlled process, is observed at peak potential and the nondiffusion-controlled process due to surface reaction associated with charge separation dominates the rest of the potentials. The $V_2O_5$ anchored CNTs exhibit a total charge storage of 2780 C/g originating from faradaic and nonfaradaic processes out of which 925 C/g (257 mAh/g that is insertion of 1.7 Li per mole of $V_2O_5$) corresponds to lithium intercalation into $V_2O_5$ layers and 1855 C/g corresponds to charge storage due to surface reaction. The innermost shaded area in Figure 5b represents the double layer capacitance contribution of bare CNTs that accounts for the value of about 690 C/g. Although direct comparison like this may not hold good truly as the CNT surface after $V_2O_5$ coating is different, there can be sufficient areas where CNTs do not have $V_2O_5$ surface. Hence, the overall charge storage associated with $V_2O_5$ surface alone at least accounts for 1165 C/g as the CNT contribution is overestimated.

It is important to investigate the origin of huge capacitive charge storage and the actual electrochemical surface area leading to overall charge storage in $V_2O_5$/CNT. The overall or total charge storage is determined using a procedure developed by Trasatti et al.[36] The procedure involves determining maximum charge that can be stored ($q^*$) in the material from the intercept

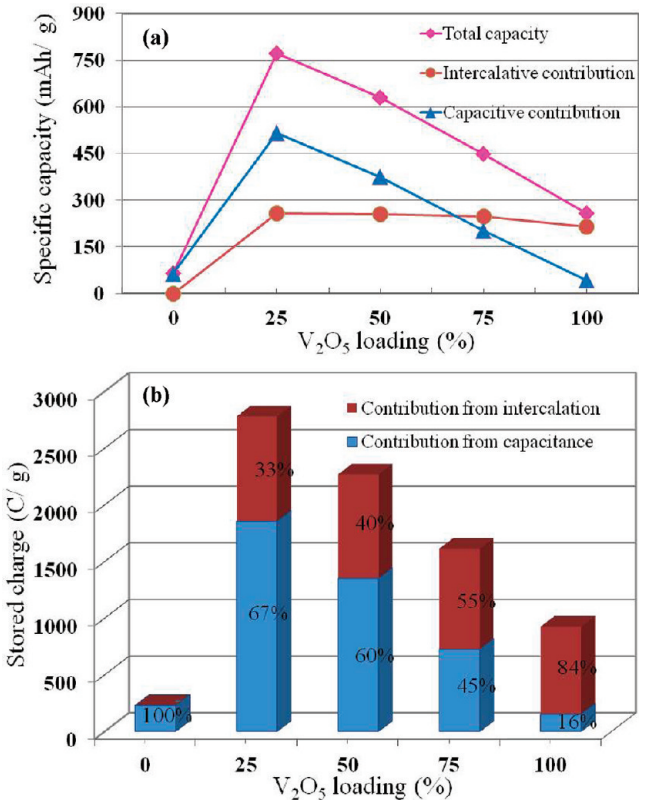


**Figure 6.** Gravimetric energy storage with $V_2O_5$/CNT electrode. (a) Plot of total specific capacity together with capacity contribution due to diffusion-controlled intercalation and capacity due to pseudocapacitance as a function of percentage $V_2O_5$ loading. (b) Bar chart showing total stored charges in C/g together with percentage contribution from capacitive and intercalation as a function of percentage $V_2O_5$ loading. All of the values shown here are calculated using CV recorded at a 0.1 mV/s scan rate.

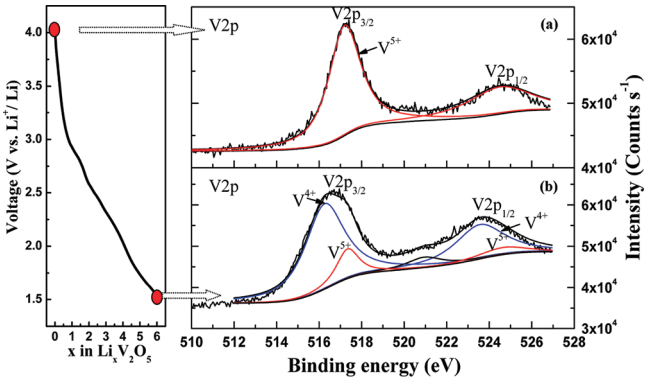


**Figure 7.** X-ray photoelectron spectra of V (2p) region of $V_2O_5$/CNT electrode after electrochemical reduction to 1.5 V in comparison with initial state. (a) The V (2p) binding energy region showing spin orbit splitting of $2P_{3/2}$ and $2P_{1/2}$ showing $V^{5+}$ state. (b) The V (2p) binding energy region of electrochemically reduced electrode showing broad V (2p) spectrum, which is deconvoluted into sets of $2P_{3/2}$ and $2P_{1/2}$ of $V^{5+}$ and $V^{4+}$ states. The discharge curve for $V_2O_5$/CNT versus Li cell used here is given on the left.

of the linear plot $1/q^*$ versus $\nu^{1/2}$. It can be also used for determining the charge stored only at the outer surface ($q_o^*$) from the intercept of the linear plot $q^*$ versus $\nu^{-1/2}$. The graphs and its descriptions are given in Supporting Information Figure S-7. The values derived from the intercept for maximum or total charge stored and charge stored at the outer surface are 2987 and 1720 C/g, respectively. The charge stored in the inner surface ($q_i^*$) is the difference between total charge ($q_t^*$) and charge stored on outer surface ($q_o^*$), which accounts for 1267 C/g.

It is worth mentioning that at high rates the nondiffusion-controlled pseudocapacitive behavior dominates intercalation capacity and vice versa as deduced from the values calculated for different scan rates given in Table S-1 of the Supporting Information. The electrochemical performance for nonsupported $V_2O_5$ xerogels, as reported in the literature, has shown either normal Li-intercalation[37] or supercapacitive properties.[32] The present results illustrate that anchoring $V_2O_5$ to CNT's surface enables high charge storage capabilities by cumulating both capacitive and faradaic processes. Therefore, at this juncture, it is important to establish how the amount of $V_2O_5$ loading and thickness of $V_2O_5$ layers over CNTs will affect the percentage contribution of intercalation and pseudocapacitance to the overall charge storage. The electrochemical performance for various grown $V_2O_5$/CNTs composites having varying amounts of $V_2O_5$ loading is measured, and the overall charge partition between insertion and redox pseudocapacitance is shown in Figure 6a and b. An increase in $V_2O_5$ loading is found to have little effect on the insertion capacitance, which remains almost unchanged with values around 260−270 mAh/g as shown in Figure 6a. By contrast, with increased $V_2O_5$ loading (the film thickness deposit), the overall surface area decreases so that the charge storage is due to the surface reaction. Accordingly, by using the elaboration of $V_2O_5$/CNTs composites, one can tune the electrode material to a desired combination of capacitive versus faradaic charge storage. This could present a positive asset for specific applications.

To further expand on the partition between the capacitive and faradaic components in $V_2O_5$/CNTs composites, an attempt is made to access changes in the oxidation state of vanadium oxide before and after the Li-ion intercalation by X-ray photoelectron spectroscopy (XPS). The measurements are done on a $V_2O_5$/CNT electrode having 25% $V_2O_5$ loading, which is discharged to 1.5 V. The XPS survey spectrum given as Supporting Information in Figure S-9 indicates considerable intensity of Li (1s) along with V (2p) and C (1s), O (1s), P (2s, 2p), and F (1s) peaks (P, F peaks coming from electrolyte and SEI). XPS of Li (1s) region is also shown in Figure S-10 of the Supporting Information. The Li (1s) peak appearing around 56.1 eV is typical of intercalated $Li^+$ in $V_2O_5$ layers.[28] The intensity of Li (1s) is feeble due to the low photoionization cross-section of Li. The V (2p) spectrum for the pristine and the electrochemically reduced electrode along with the discharge curve are shown in Figure 7.

It is found that the electrochemically reduced sample shows significant broadening of the XPS peaks, indicating the presence of multiple components. The broad peak can be deconvoluted into two peaks of $2p_{3/2}$ at 516.25 and 517.33 eV together with $2p_{1/2}$ at 523.55 and 524.63 eV corresponding to $V^{4+}$ and $V^{5+}$ states, respectively.[38] The broad peak at 520.95 eV is attributed to the satellite arising due to the multiple oxidation states of vanadium.[38]

The deconvoluted peak positions, intensity, and fwhm are given in Table S-2 of the Supporting Information. The concentration ratio of $V^{5+}$:$V^{4+}$ calculated from V(2p) spectrum is about 15:85. From simple calculations, the capacity associated with the

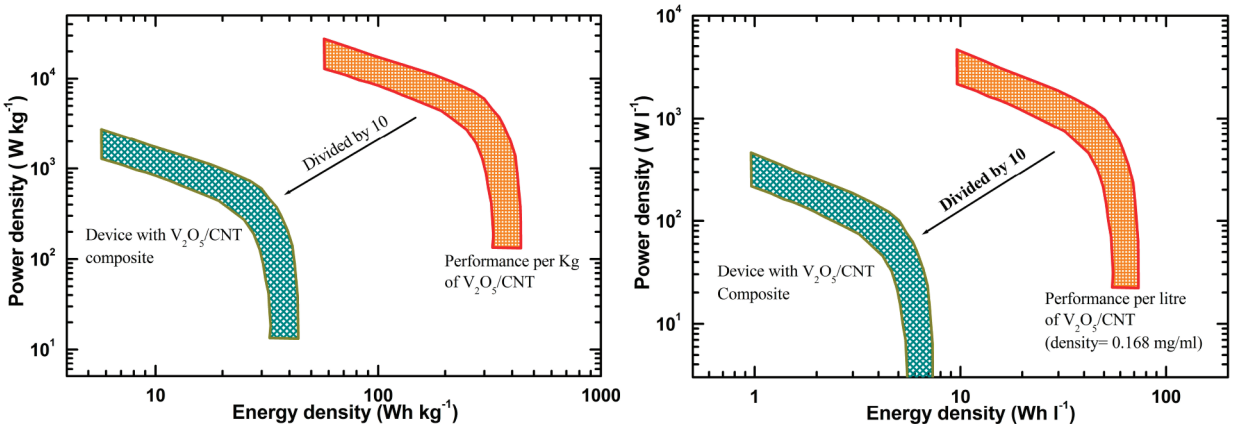


**Figure 8.** Ragone plot showing gravimetric and volumetric energy and power density of $V_2O_5$/CNT battery hybrid supercapacitor electrode. The total weight of $V_2O_5$ loading along with CNT weight is used here for energy and power density calculations.

reduction of 85% of $V^{5+}$ to $V^{4+}$ (e.g., insertion of 1.7 $Li^+$ in $V_2O_5$) equated to 257 mAh/g, which is nearly similar to the Li insertion contribution (Figure 6) determined from exploitation of the voltammetry data. This result implies an insertion capacity of about 925 C/g associated with the $V^{5+}/V^{4+}$ redox couple. This is in agreement with previous XPS measurements on various $V_2O_5$ specimens, which fail to reveal any change in the V oxidation states, while the samples show large capacitances.[33] Nevertheless, the origin of the large capacity (~1850 C/g) due to the nondiffusion-controlled process remains to be explained.

At this juncture, to complete the discussion, we must address the origin of huge nonfaradaic (double layer) capacitance observed with $V_2O_5$/CNT composites, bearing in mind early literature dealing with charge storage mechanisms in $V_2O_5$ aeorogels or $MnO_2$ as discussed by Dunn et al.[39] and Ruetschi,[40] respectively. The proposed mechanisms are nested in the presence of 3d metal vacancies, which act as "holders" for neighboring cationic charges either as $H^+$ or as $Li^+$, so as to maintain local electroneutrality, the end result being the trapping of either $Li^+$ or $H^+$ near cation vacancies without electron transfer to the adjacent cation. We believe that a similar mechanism prevails here as well and can be used to account for the 1165 C/g surface capacitance experimentally measured on $V_2O_5$/CNT composites. It is noteworthy that charges stored on the outer surface and calculated by using the Trasatti procedure (1720 C/g) indicate that cation vacancies are concentrated on the surface.

Finally, the best way to give a realistic picture of high power and high energy density exhibited with $V_2O_5$-anchored CNT hybrid is to plot our results as a conventional Ragone plot (Figure 8a). Bearing in mind practical aspects, we measured the tap densities of our 25%$V_2O_5$/CNT composite to be equal to 0.168 g/mL. On the basis of these values and the use of 2 mg/$cm^2$ electrode loading, we could plot both volumetric and gravimetric (specific) power for our composite electrode. Performance of the corresponding supercapacitor devices will depend upon the nature of the counter electrode and on the type of selected configuration asymmetric or symmetric albeit with the need to polarize the two electrodes prior to cell assembly for the symmetric configuration for which $C_{dev} = C_{elec}/2$. For all aforesaid reasons, and because we have only 2 mg of loaded electrode, we applied a conservative correction factor of 10 to perform our calculation while the rule of thumb is usually 3.5. Despite such a correction factor, although caution must be exercised, $V_2O_5$−CNT composites still compare favorably with commercial carbon EDLC supercapacitors carbon electrodes, which for similar loading give about 6−7 times lesser energy density (~10 Wh/kg as compared to ~70 Wh/kg), further suggesting the benefits of using electrode architectures cumulating both intercalation capacity and redox pseudocapacitance.

Finally, a legitimate question arises on the origin of the widespread charge storage values ranging between 300 and 800 mAh/g reported for $V_2O_5$ aerogels. Dunn's recent work,[15] dealing with charge storage capabilities of mesoporous transition metal oxides having oriented layered nanocrystalline domains, could provide an answer to this question. Indeed, the authors have shown an enhanced capacitance for crystalline as compared to amorphous mesoporous samples, the explanation being that the overall capacity arises from an intercalation capacitance associated with the insertion of Li within the interlayer gap of the oxides. A similar explanation could hold in our case for $V_2O_5$, because according to the grafting mechanism, layers of $V_2O_5$ grow epitaxially parallel to the CNT surface forming thin films of 4−5 nm containing 8−10 stacked $V_2O_5$ layers. Such a nanostructuring provides (i) a very short diffusion path for the ions coming from the electrolyte, and (ii) an easy access to the gap within layers for Li insertion, enabling the feasibility of having a rapid insertion capacitance associated with the reduction of $V^{4+}$ and $V^{5+}$. Along that line, as both the crystalline nature and the nucleation growth direction for the $V_2O_5$ specimens influence the electrochemical performances, it does not come as a surprise that reported capacities can be so spread, rendering comparative studies difficult. Nevertheless, it should be mentioned that a recent study,[41] carried out in an aqueous medium, has also shown an enhancement in the capacitance of electrodes made of $V_2O_5$ electrodeposited on carbon nanofibers, which confirms the importance of the electrode structuring.

## ■ CONCLUSIONS

$V_2O_5$/CNT hybrid is attractive for electrochemical energy storage due to its relatively high emf (about 4 V vs $Li/Li^+$) and accommodation of a large amount of lithium, which results in a surprisingly high specific capacity of 850 mAh/g as compared to 350 mAh/g for classical $V_2O_5$ powder electrode. The origin of such large specific capacity is explained through an arsenal of

analytical techniques and previously reported models as the cumulative effect of insertion and pseudocapacitance. Rational design of such composition possessing insertion and pseudocapacitance offers the possibility of tailoring the power and energy density of electrode material. However, limited cyclability remains the major problem of such materials, especially when made at the nanoscale, due to the dissolution of the active material during the charge−discharge process. Use of ionic liquids and specific electrolyte additives may help in circumventing the problem of vanadium dissolution and thereby in achieving stable capacity. Accordingly, a promising research direction lies in prospecting more robust oxides toward dissolution.

## METHODS

The CNT−$V_2O_5$ composites were prepared as follows. About 500 mg of prefunctionalized carbon nanotubes (10−30 nm) (Aldrich make) was suspended in about 50 mL of absolute ethanol by sonicating for 30 min. Functionalization of CNTs was carried out using a procedure reported elsewhere.[42] 0.5 mL of vanadium oxytripropxide (99% purity, Aldrich make) was added to the suspension, and the resulting mixture was continuously stirred for 1 day. Stirring is continued with addition of 0.1 mL of distilled water at regular intervals to allow the slow hydrolysis of vanadium oxy tripropoxide. The total water to vanadium oxytripropoxide ratio is maintained greater than 10 to ensure complete hydrolysis. The reactants taken above correspond to a weight ratio of $V_2O_5$:CNT of 75:25. Surplus amount of absolute ethanol used during the synthesis is to avoid instant hydrolysis of vanadium oxytripropxide. After 48 h of stirring, the resulting gel was aged for a week, washed with acetone, and allowed to dry at room temperature. Finally, the composites were dried at 200 °C and used for further characterization. For comparison, unsupported $V_2O_5$ xerogel was prepared following the above procedure by maintaining the same conditions, but without the addition of carbon nanotubes. The $V_2O_5$ loading of 50 and 75 wt % on CNTs was also prepared. Yet the 25 wt % $V_2O_5$/CNT is mainly used for all of the characterization and electrochemical measurements unless otherwise mentioned.

**Characterization.** Powder X-ray diffraction patterns of the prepared samples were recorded using an X'pert PRO-PANalytical diffractometer with Cu $K_\alpha$ radiation. Vanadium oxide thin coating over carbon nanotube was investigated using a Technai-20 $G_2$ transmission electron microscope. Scanning electron microscopy images were obtained with FESEM. X-ray photoelectron spectra were recorded on a ESCA lab-2000 spectrometer equipped with Al $K_\alpha$ source.

**Electrochemical Measurements.** Electrochemical tests were carried out on Swagelok-type cells assembled in an argon-filled glovebox. The $V_2O_5$/CNT constituted the positive electrode of the half cell with a metallic lithium counter electrode. 1 mol/L $LiClO_4$ dissolved in a mixture of 1:1 volume percent ethylene carbonate and dimethyl carbonate was used as electrolyte. The electrochemical experiment was conducted using VMP3Z (Biologica) multichannel potentiostat/galvanostat.

The constant power experiments were conducted on $V_2O_5$/CNT composite electrode versus Li metal anode in a typical two-electrode coin cell. The constant power (current is applied such that at any given time, current × voltage is constant) corresponding to 50−1500 W/kg in intervals of 50 W is applied, and the time to reach the cutoff potential is measured. Energy is derived from time × power.

## ASSOCIATED CONTENT

**Supporting Information.** Ten figures and two tables showing structure of $V_2O_5$, characterization data, and electrochemical analysis of $V_2O_5$/CNT composite electrode. This material is available free of charge via the Internet at http://pubs.acs.org.

## AUTHOR INFORMATION

**Corresponding Author**
prakash.as@gmail.com

## ACKNOWLEDGMENT

The financial support from the EMPOWER Scheme (DU-01 OLP-0062) of Council of Scientific and Industrial Research, New Delhi, India, is gratefully acknowledged. M.S. thanks CSIR for granting a Senior Research Fellow. Thanks are due to Prof. Patrice Simon for helpful discussions and valuable input. Prof. M. S. Hegde (IISc, Bangalore) is warmly thanked for extending the XPS facility, Dr. Parthasarathy Bera (NAL, Bangalore) for assistance on XPS analysis, Dr. Shivan (Icon analyticals) for assistance on TEM studies, and Mr. Nilesh Tripati (NIT, Warangal & JNCASR Summer research fellow 2008) for assistance in initial experiments.

## REFERENCES

(1) Abraham, K. M.; Jiang, Z. *J. Electrochem. Soc.* **1996**, *143*, 1–5.
(2) Ogasawara, T.; Debart, A.; Holzapfel, M.; Novak, P.; Bruce, P. G. *J. Am. Chem. Soc.* **2006**, *128*, 1390–1393.
(3) Girishkumar, G.; McCloskey, B.; Luntz, A. C.; Swanson, S.; Wilcke, W. *J. Phys. Chem. Lett.* **2010**, *1*, 2193–2203.
(4) Simon, P.; Gogotsi, Y. *Nat. Mater.* **2008**, *7*, 845–854.
(5) Lang, X.; Hirata, A.; Fujita, T.; Chen, M. *Nat. Nanotechnol.* **2011**, *6*, 232–236.
(6) Stoller, M. D.; Park, S.; Zhu, Y.; An, J.; Ruoff, R. S. *Nano Lett.* **2008**, *8*, 3498–3502.
(7) Cui, L.-F.; Ruffo, R.; Chan, C. K.; Peng, H.; Cui, Y. *Nano Lett.* **2009**, *9*, 491–495.
(8) Bruce, P. G.; Scrosati, B.; Tarascon, J.-M. *Angew. Chem., Int. Ed.* **2008**, *47*, 2930–2946.
(9) Binotto, B.; Larcher, D.; Prakash, A. S.; Urbina, R. H.; Hegde, M. S.; Tarascon, J.-M. *Chem. Mater.* **2007**, *19*, 3032–3040.
(10) Wang, H.; Cui, L.-F.; Yang, Y.; Casalongue, H. S.; Robinson, J. T.; Liang, Y.; Cui, Y.; Dai, H. *J. Am. Chem. Soc.* **2010**, *132*, 13978–13980.
(11) Bi, R.-R.; Wu, X.-L.; Cao, F.-F.; Jiang, L.-Y.; Guo, Y.-G.; Wan, L.-J. *J. Phys. Chem. C* **2010**, *114*, 2448–2451.
(12) Wang, Y.; Zhitomirsky, I. *Langmuir* **2009**, *25*, 9684–9689.
(13) Chen, Z.; Augustyn, V.; Wen, J.; Zhang, Y.; Shen, M.; Dunn, B.; Lu, Y. *Adv. Mater.* **2011**, *23*, 791–795.
(14) Wang, Y.; Cao, G. *Adv. Mater.* **2008**, *20*, 2251–2269.
(15) Brezesinski, T.; Wang, J.; Tolbert, S. H.; Dunn, B. *Nat. Mater.* **2010**, *9*, 146–151.
(16) Enjalbert, R.; Galy, J. *Acta Crystallogr.* **1986**, *C42*, 1467–1469.
(17) Petkov, V.; Trikalitis, P. N.; Bozin, E. S.; Billinge, S. J. L.; Vogt, T.; Kanatzidis, M. G. *J. Am. Chem. Soc.* **2002**, *124*, 10157–10162.
(18) Dong, W.; Sakamoto, J. S.; Dunn, B. *Sci. Technol. Adv. Mater.* **2003**, *4*, 3–11.
(19) Ajayan, P. M. *Chem. Rev.* **1999**, *99*, 1787–1799.
(20) Tasis, D.; Tagmatarchis, N.; Bianco, A.; Prato, M. *Chem. Rev.* **2006**, *106*, 1105–1136.
(21) Salvetat, J.-P.; Bonard, J.-M.; Thomson, N. H.; Kulik, A. J.; Forró, L.; Benoit, W.; Zuppiroli, L. *Appl. Phys. A: Mater. Sci. Process.* **1999**, *69*, 255–260.
(22) Eder, D. *Chem. Rev.* **2010**, *110*, 1348–1385.
(23) Lin, Y.; Watson, K. A.; Fallbach, M. J.; Ghose, S.; Smith, J. G., Jr.; Delozier, D. M.; Cao, W.; Crooks, R. E.; Connell, J. W. *ACS Nano* **2009**, *3*, 871–884.

(24) Liu, R.; Duaya, W. J.; Lee, S. B. *Chem. Commun.* **2011**, *47*, 1384–1404.
(25) Gao, C.; Li, W.; Morimoto, H.; Nagaoka, Y.; Maekawa, T. *J. Phys. Chem. B* **2006**, *110*, 7213–7220.
(26) Livage, J. *Solid State Ionics* **1996**, *86−88*, 935–942.
(27) Livage, J. *Chem. Mater.* **1991**, *3*, 578–593.
(28) Ibris, N.; Salvi, A. M.; Liberatore, M.; Decker, F.; Surca, A. *Surf. Interface Anal.* **2005**, *37*, 1092–1104.
(29) Legrand, D. L.; Nesbitt, H. W.; Bancroft, G. M. *Am. Mineral.* **1998**, *83*, 1256–1265.
(30) Moulder, J. F.; Stickle, W. F.; Sobol, P. E.; Bomben, K. D. *Handbook of X-ray Photoelectron Spectroscopy*; Perkin Elmer Corp., Physical Electronics Division: Minnesota, 1992.
(31) Conway, B. E. *J. Electrochem. Soc.* **1991**, *138*, 1539–1548.
(32) Kim, II-H.; Kim, J.-H.; Cho, B.-W.; Lee, Y. H.; Kim, K. B. *J. Electrochem. Soc.* **2006**, *153*, A989–A996.
(33) Passerini, S.; Le, D. B.; Smyrl, W. H.; Barrettoni, M.; Tossici, R.; Marassi, R.; Giorgetti, M. *Solid State Ionics* **1997**, *104*, 195–204.
(34) Lindstrolm, H.; Soldergren, S.; Solbrand, A.; Rensmo, H.; Hjelm, J.; Hagfeldt, A.; Lindquist, S. E. *J. Phys. Chem. B* **1997**, *101*, 7717–7722.
(35) Wang, J.; Polleux, J.; Lim, J.; Dunn, B. *J. Phys. Chem. C* **2007**, *111*, 14925–14931.
(36) Ardizzone, S.; Fregonara, G.; Trasatti, S. *Electrochim. Acta* **1990**, *35*, 263–267.
(37) Le, D. B.; Passerini, S.; Tipton, A. L.; Owens, B. B.; Smyrl, W. H. *J. Electrochem. Soc.* **1995**, *142*, L102–L103.
(38) Silversmit, G.; Depla, D.; Poelman, H.; Marin, G. B.; Gryse, R. D. *J. Electron Spectrosc. Relat. Phenom.* **2004**, *135*, 167–175.
(39) Rolison, D. R.; Dunn, B. *J. Mater. Chem.* **2001**, *11*, 963–980.
(40) Ruetschi, P. *J. Electrochem. Soc.* **1984**, *131*, 2737.
(41) Ghosh, A.; Ra, E. J.; Jin, M.; Jeong, H. K.; Kim, T. H.; Biswas, C.; Lee, Y. H. *Adv. Funct. Mater.* **2011**, *21*, 2541–2547.
(42) Osorio, A. G.; Silveira, I. C. L.; Bueno, V. L.; Bergmann, C. P. *Appl. Surf. Sci.* **2008**, *255*, 2485–2489.